Rock and Soil Mechanics

Volume 42 | Issue 9 Article 5

12-14-2021

Analysis of catastrophic instability of roof-rib pillar support system under backfill mining

Xuan-ting LIU
University of Chinese Academy of Sciences, Beijing 100049, China

Cong-xin CHEN
University of Chinese Academy of Sciences, Beijing 100049, China

Xiu-min LIU
University of Chinese Academy of Sciences, Beijing 100049, China

Kai-zong XIA
University of Chinese Academy of Sciences, Beijing 100049, China, kzxia@whrsm.ac.cn

See next page for additional authors

Custom Citation

LIU Xuan-ting, CHEN Cong-xin, LIU Xiu-min, XIA Kai-zong, ZHANG Chu-qiang, WANG Tian-long, WANG Yue, . Analysis of catastrophic instability of roof-rib pillar support system under backfill mining[J]. Rock and Soil Mechanics, 2021, 42(9): 2461-2471.

Analysis of catastrophic instability of roof-rib pillar support system under backfill mining

Authors

Xuan-ting LIU, Cong-xin CHEN, Xiu-min LIU, Kai-zong XIA, Chu-qiang ZHANG, Tian-long WANG, and Yue WANG

Rock and Soil Mechanics 2021 42(9): 2461−2471 ISSN 1000−7598
https: //doi.org/10.16285/j.rsm.2021.5453 rocksoilmech.researchcommons.org/journal

Analysis of catastrophic instability of roof-rib pillar support system under backfill mining

LIU Xuan-ting[1, 2], CHEN Cong-xin[1, 2], LIU Xiu-min[1, 2], XIA Kai-zong[1, 2], ZHANG Chu-qiang[3], WANG Tian-long[1, 2], WANG Yue[1, 2]

1. State Key Laboratory of Geomechanics and Geolechnical Engineering, Institute of Rock and Soil Mechanics, Chinese Academy of Sciences, Wuhan, Hubei 430071, China

2. University of Chinese Academy of Sciences, Beijing 100049, China

3. School of Civil Engineering, Architecture and Environment, Hubei University of Technology, Wuhan, Hubei 430068, China

Abstract: A roof−rib pillar support system is often formed in the metal mines that applied to the backfill mining method. In order to ensure the safe mining, it is of great significance to explore the failure mechanism of the roof−rib pillar support system under backfill mining. On the basis of considering the side pressure effect of the backfill on the rib pillar, a mechanical model of the roof−rib pillar support system under backfill mining was established. Furthermore, the catastrophe theory was used to explore the failure mechanism of the supporting system under the action of the filling body, and the influence of the structural parameters of the support system before and after filling on the stability of the stope was analyzed. The research results show that under the condition of certain mechanical properties of the rock mass, the stability of the roof−rib pillar support system under backfill mining is controlled by the stope structure parameters (roof thickness, stope span, rib pillar width, rib pillar height), the overburden load and the side pressure of the backfill. The addition of the filling body will reduce the stiffness ratio of the support system, thereby improving the stability of the stope. When the stope is at an unfilled state, the optimization sequence of the structural parameters of the support system should be roof thickness, stope span, rib pillar width and rib pillar height. When the stope is at the state of filling, the optimization sequence should be roof thickness, rib pillar width, stope span, and rib pillar height. The combination of theoretical derivation and numerical simulation is applied in the supporting project to verify the correctness of theoretical derivation.

Keywords: mining engineering; filling; catastrophe theory; roof; rib pillar; stope stability

1 Introduction

The backfill mining method has irreplaceable advantages in improving the recovery rate and stope stability, and controlling surface subsidence. In recent years, the backfill mining method has been widely applied in metal mines[1]. For metal mines that use the backfill mining method, a roof−rib pillar support system will be formed in the actual production process. For a specific metal mine, the mechanical properties of the rock mass are fixed, and the stability of the support system mainly depends on the structural parameters of the stope. Most metal mines often use empirical equation to optimize stope structure parameters[2]. However, the selected parameters are often found not to meet the production requirements. On one hand, the recovery rate will be reduced, which will affect the economic benefits of the mine if the design of parameters is too conservative. On the other hand, it will lead to instability and destruction of the stope, thus affecting the safety production of the stope. Therefore, the studies on the instability and failure mechanism of the roof−rib pillar support system under backfill mining are of great significance to the safe and efficient mining of such metal mines.

Many studies related with the stability of such metal mines can be found. Xie et al.[3] studied the influence of the elastic coefficient of cemented backfill and the un-topped height on stope stability. Xu et al.[4] established an evaluation method of irregular stope stability by using the Voronoi diagram method. Verma et al.[5] used both the empirical formula method and numerical simulation method to analyze the stability of high and narrow coal pillar−roof support system. Wang et al.[6] combined the nonlinear regression method and numerical simulation method to established the prediction equation of critical thickness of stage considering the influence of combined factors. It can be seen that many scholars have done a lot of research works on the stability of the roof−rib pillar support system, but most of them focus on qualitative

Received: 31 March 2021 Revised: 14 May 2021
This work was supported by the Young Scholar Fund of National Natural Science Foundation of China(42002292).
First author: LIU Xuan-ting male, born in 1995, PhD candidate, focusing on surface rock movement and underground mining stability.
E-mail: liuxuanting18@mails.ucas.ac.cn
Corresponding author: XIA Kai-zong, male, born in 1988, PhD, Assistant Professor, research interests: underground mining stability and slope stability. E-mail: kzxia@whrsm.ac.cn

analysis of ideal elasticity.

Considering that the instability and failure of the roof−rib pillar support system was a complex nonlinear problem, the catastrophe theory was applied to study stope stability. The good application results were achieved[7−8]. Xia et al.[9] applied catastrophe theory to analyze the damage of the top layer−pillar support system in the gypsum mine, furthermore, the influence of relative humidity on stope stability was considered. Ren et al.[10] constructed a three-dimensional mechanical model of the roof−pillar support system under backfill mining. Both the catastrophe and creep theories were applied to clarify the instability failure mechanism of the goaf group from the perspective of energy conversion. Xu et al.[11] applied the cusp catastrophe theory to analyze the mechanical mechanism of stope instability by analyzing the formation and failure mechanism of the roof structure of the filling stope. Qi[12] carried out a secondary development in FLAC^{3D} based on the FISH language on the energy basis, and used strength reduction and cusp mutation methods to check the safety factor of the filling stope support system. Xu et al.[13] established a pre-warning model for instability of filling body based on the cusp catastrophe theory and considered the energy evolution characteristics.

For metal mines that adopt the backfill method, in order to improve the stability of the stope, the goaf is often filled in time. Zhu[14] and Kostecki[15] found that the side pressure of the filling body can increase the strength of the adjacent rib pillars, thereby improving the stability of the stope. In this paper, a simplified mechanical model of the roof−rib pillar support system under the action of the filling body was established. Furthermore, a cusp catastrophe model of the roof−rib pillar support system considering the lateral pressure of the filling body was constructed. This model is used to explore the failure mechanism of the roof−rib pillar support system under backfill mining, and the results are applied in a metal mine of northeastern China.

2 Mechanical model

In metal mines that use the backfill mining method, it is necessary to reserve a roof to carry the overlying load. When the ore body has a large span, pillars are usually left in the middle of the stope to reduce the stope span. In the actual mining process, in order to improve the stability of the stope, the goaf will be filled in time. Therefore, a roof−rib pillar support system under backfill mining is shown in Fig.1.

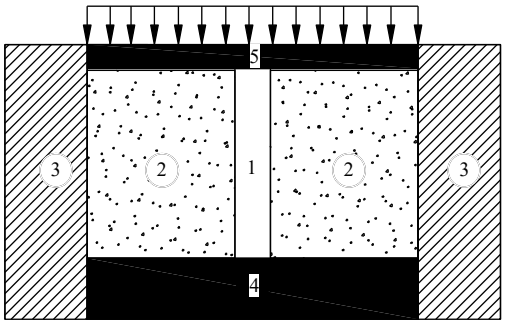

①Rib pillar; ②Filling body; ③Surrounding rock; ④Sill pillar; ⑤Roof

Fig. 1 Schematic diagram of support system

The analysis of underground stope stability is a complex mechanical problem. In the case of reflecting the mechanical nature of the research problem, some simplifications are made as follows. The length of the stope in the strike direction is much larger than the width in the vertical strike direction, thus the complex three-dimensional mechanical problems can be transformed into two-dimensional plane problems. Considering that the surrounding rock has a good restraining effect on the roof, the roof is simplified as an elastic rock beam with the bending strength EI and is fixed at both ends. The overlying load q is simplified as uniformly distributed load. The effect of the rib pillars on the roof can be regarded as the concentrated force F. Since the displacement of the rib pillars is much larger than that of the stope sill pillars, it is assumed that the stope sill pillar is rigid. The addition of the filling body can exert lateral pressure on the rib pillars, thereby improving the stress state and strength of the rib pillars, which play a major bearing role in the supporting system. Therefore, this paper only considers the supporting effect of the pillar under the lateral pressure of the filling body on the roof, which is consistent with the experimental model of Song et al.[16]. In summary, the mechanical model of the roof−rib pillar support system under the action of the filling body is established as shown in Fig.2.

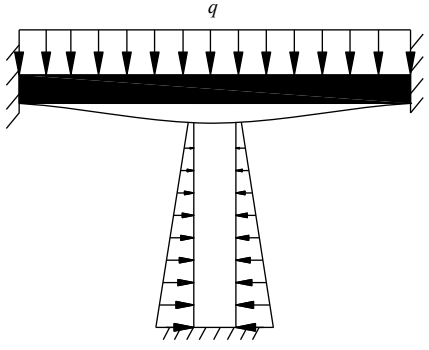

Fig. 2 Simplified mechanical model of support system

3 Stress−strain relationship of rib pillar under the action of backfill

According to damage mechanics, Weibull distribution has strong applicability in describing the stress−strain relationship of the rib pillar[17].

$$\sigma = E_0 \varepsilon \exp\left[-\left(\frac{\varepsilon}{\varepsilon_0}\right)\right]^m \quad (1)$$

where σ is the stress of the rib pillar; E_0 is the initial elastic modulus of the rib pillar; ε is the compressional strain; ε_0 is the average strain; and m is the shape parameter in the Weibull distribution.

Donovan et al.[18] considered the roughness of the contact surface in the goaf and the unloading deformation of the goaf to squeeze the filling body, and proposed that the lateral pressure of the filling body on the rib pillar satisfies the following:

$$\sigma_h = \gamma h K_p + 2c\sqrt{K_p} + q_0 K_p \quad (2)$$

where γ is the weight of the filling body; h is the height of the filling body; K_p is the earth pressure coefficient, which can be corrected according to Table 1; c is the cohesion of the filling body; and q_0 is the load acting on the filling body.

Table 1 Earth pressure coefficient correction

Internal friction angle of the filling body /(°)	25	30	35	40	45
Earth pressure coefficient	4.29	6.42	10.2	17.3	33.5

The damage of the rib pillars is an integral instability problem. In order to simplify the analysis, the parameters in Table 2 are substituted into Eq. (1). It can be estimated that the equivalent lateral pressure of the filling body on the lateral pressure of the rib pillar is about 5 MPa. Fig.3 shows the standard rib pillar samples obtained from the engineering site. In order to obtain the stress−strain curve of the rib pillar under the side pressure of the filling body, the INSTRON-1346 rigid electro-hydraulic servo testing machine shown in Fig.4 was used to compare the confining pressure of the rib pillar specimen with the equivalent lateral pressure (5 MPa). A triaxial test was carried out to simulate the influence of the addition of the filling body on the stress−strain relationship of the rib pillars. Figs. 5(a) and 5(b) show the stress−strain tests and fitting curves of the rib pillar specimens under different confining pressure states, which represent the mechanical characteristics of the rib pillar at the unfilled and filled states, respectively. It can be seen from Fig.5 that the Weibull distribution can better describe the stress−strain relationships between the unfilled state and the filled state of the rib pillar specimen. The addition of equivalent lateral pressure changes the stress state of the rib pillar. The peak strength and peak strain of the rib pillar specimen are significantly increased, and the post−peak curve of the rib pillar specimen transfers from brittleness to ductility. Many scholars have also verified the above phenomena through the in situ monitoring[19] and model tests[20], which prove that it is reasonable to use equivalent lateral pressure to simulate the influence of the filling body on the constitutive relationship of the rib pillar.

Table 2 The mechanical parameters of the filling body and the height of stope

Types	Density /(kg • m^{-3})	Cohesion /MPa	Internal friction angle /(°)	Height of stope /m
Filling body	1 970	0.24	31	—
Parameters of stope	—	—	—	80

Fig. 3 Rib pillar samples

Fig. 4 Rigid electro-hydraulic servo testing machine

After the filling body is added, the initial elastic modulus E_0 is increased from 27.02 MPa to 28.70 MPa, and the average strain ε_0 is increased from 11.25×10^{-3} to 13.28×10^{-3}, while the shape parameter m decreases from 2.98 to 1.98. The initial elastic modulus E_0 remains

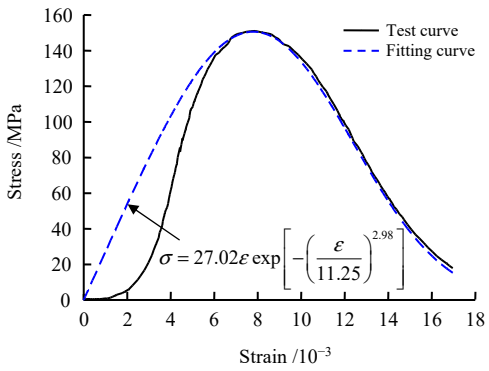

(a) Unfilled state: no equivalent confining pressure is applied

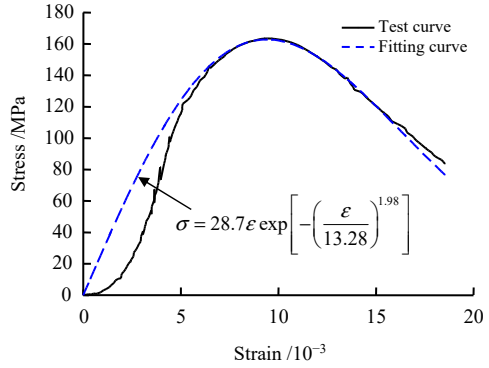

(b) Filled state: equivalent confining pressure is applied

Fig. 5 Stress−strain test and fitting curves of rib−pillar specimens under different confining pressures

basically unchanged before and after filling. The lateral pressure of the filling body mainly affects the average strain ε_0 and the shape parameter m. Therefore, the constitutive relationship of the rib pillar under the action of the filling body can be written as

$$\sigma = E_0\varepsilon \exp\left[-\left(\frac{\varepsilon}{k_1\varepsilon_0}\right)^{k_2 m}\right] \tag{3}$$

where k_1 and k_2 are the impact coefficients of the filling body on the average strain ε_0 and the shape parameter m of the rib pillar, respectively. When the rib pillar is at the unfilled state, both k_1 and k_2 are equal to 1. The side pressure of the filling body will cause k_1 to increase and k_2 to decrease.

Taking the unit length in the strike direction of the roof and the isolation pillar as the study object, the width of the pillar is B, and the height of the pillar is H. The load−deformation relationship of the rib pillar at the filled state is

$$F = \sigma A = \frac{E_0 B}{H} u \exp\left[-\left(\frac{u}{k_1 u_0}\right)^{k_2 m}\right] = \lambda u \exp\left[-\left(\frac{u}{k_1 u_0}\right)^{k_2 m}\right] \tag{4}$$

where A is the cross-sectional area of the rib pillar; $\lambda = E_0B/H$, is the initial stiffness; u is the compressional displacement of the rib pillar at the filled state; and u_0 is the compressional displacement corresponding to the peak load at the filled state.

4 Deflection curve equation of rock beam

Based on the simplified mechanical model established above, the roof can be regarded as an elastic rock beam fixed at both ends and supported by the supporting force F of the rib pillar in the middle. Because the stiffness of the filling body is low, the influence of the addition of the filling body on the sinking of the roof is ignored. Under the action of the overburden load and the supporting force of the rib pillar, it is assumed that the compression displacement u of the rib pillar is equal to the deflection of the roof at the midpoint (see Fig.6). Using the displacement method in structural mechanics, the bending moment M_{AB} at the beam end and the shear force Q_{AB}[21] can be solved (the lateral pressure on the beam cross section is assigned as positive affected by the bending moment).

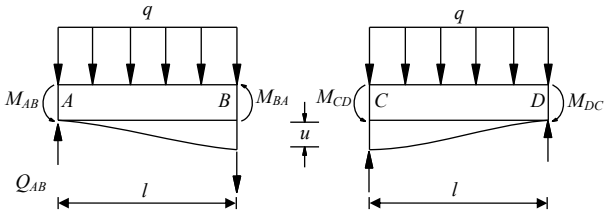

Fig. 6 Bending moment and reaction at the ends of beam

$$\left.\begin{aligned} M_{AB} &= -\frac{ql^2}{12} - \frac{6EI}{l^2}u \\ Q_{AB} &= \frac{ql}{2} + \frac{12EI}{l^3}u \end{aligned}\right\} \tag{5}$$

where E is the elastic modulus of the rock beam; I is the moment of inertia of the rock beam; and l is the stope span.

Half of the model can be studied because the model is symmetric. Taking point A as the origin, the bending moment $M(x)$ equation of section AB can be solved by Eq. (5) as

$$M(x) = M_{AB} + Q_{AB}x - \frac{qx^2}{2} = -\frac{qx^2}{2} + \left(\frac{ql}{2} + \frac{12EI}{l^3}u\right)x - \left(\frac{ql^2}{12} + \frac{6EI}{l^2}u\right) \tag{6}$$

Substituting Eq. (6) into the differential equation for deflection leads to

$$EIw'' = \frac{qx^2}{2} - \left(\frac{ql}{2} + \frac{12EI}{l^3}u\right)x + \left(\frac{ql^2}{12} + \frac{6EI}{l^2}u\right) \quad (7)$$

where w'' is the second derivative of the differential equation for deflection; and x is the distance of the point from A.

The differential equation for deflection w of section AB can be obtained by integrating Eq. (7),

$$w = \frac{qx^4}{24EI} - \left(\frac{ql}{2EI} + \frac{12u}{l^3}u\right)\frac{x^3}{6} + \left(\frac{ql^2}{12EI} + \frac{6u}{l^2}\right)\frac{x^2}{2} \quad (8)$$

5 Cusp catastrophe model and instability analysis

5.1 Potential energy function of the supporting system

Under the action of the overlying load, the roof of the supporting system will deflect and produce the bending deformation energy U_s. The compressive displacement occurs at the upper end of the rib pillar due to the action of the roof sinking, thereby generating the compressive deformation energy U_p. The lateral pressure will inhibit the generation of micro-cracks and energy dissipation in the rib pillars, thereby affecting the compression variable energy. The energy of the roof bending deformation energy U_s and compression deformation energy U_p is from the external force work W caused by the overlying load q. Based on the energy principle, the total potential energy Π of the support system is composed of the roof bending deformation energy U_s, the rib pillar compression deformation energy U_p, and the external force work W:

$$\Pi = U_s - W + U_p \quad (9)$$

The bending deformation energy of the roof is

$$U_s = EI\int_0^l [w''(x)]^2 \mathrm{d}x = EI\int_0^l \left[\frac{q^2x^4}{4} - \left(\frac{q^2l}{2} + \frac{12EIq}{l^3}u\right)x^3 + \left(\frac{q^2l^2}{3} + \frac{18EIq}{l^2}u + \frac{144E^2I^2}{l^6}u^2\right)x^2 + \left(\frac{q^2l^3}{12} + \frac{8EIq}{l^2}u + \frac{144E^2I^2}{l^5}u^2\right)x + \left(\frac{q^2l^4}{144} + EIqu + \frac{36E^2I^2}{l^4}u^2\right)\right]\mathrm{d}x = \frac{q^2l^5}{720EI} + \frac{12EI}{l^3}u^2 \quad (10)$$

The work done by external forces to the support system is

$$W = 2\int_0^l qw(x)\mathrm{d}x = qlu + \frac{q^2l^5}{360EI} \quad (11)$$

The compression deformation energy of the rib pillar is

$$U_p = \int_0^u F\mathrm{d}u = \int_0^u \lambda u \exp\left[-\left(\frac{u}{k_1u_0}\right)^{k_2m}\right]\mathrm{d}u \quad (12)$$

Combining Eqs. (9)−(12), the total potential energy of the supporting system under the action of the filling body can be obtained as

$$\Pi = \frac{12EI}{l^3}u^2 + \int_0^u \lambda u \exp\left[-\left(\frac{u}{k_1u_0}\right)^{k_2m}\right]\mathrm{d}u - qlu - \frac{q^2l^5}{720EI} \quad (13)$$

5.2 Cusp catastrophe model of support system

Using the compression displacement u as the independent variable to solve the first derivative of the total potential energy Π, set $\Pi' = 0$, the equilibrium surface equation can be written as

$$\Pi' = \frac{24EI}{l^3}u + \lambda u \exp\left[-\left(\frac{u}{k_1u_0}\right)^{k_2m}\right] - ql = 0 \quad (14)$$

Equation (14) represents the equilibrium equation of the rib pillar−roof support system under the action of the filling body. According to the smooth nature of the balance surface, the cusp catastrophe model needs to satisfy $\Pi''' = 0$ at the cusp, that is

$$\Pi''' = \frac{-\lambda k_2 m}{u_0}\exp\left[-\left(\frac{u}{k_1u_0}\right)^{k_2m}\right]\left(\frac{u}{k_1u_0}\right)^{k_2m-1} \cdot \left[1 - k_2m\left(\frac{u}{k_1u_0}\right)^{k_2m} + k_2m\right] = 0 \quad (15)$$

From Eq. (15), it can be seen that at the cusp

$$u = u_1 = k_1u_0\left(\frac{1+k_2m}{k_2m}\right)^{\frac{1}{k_2m}} \quad (16)$$

where u_1 is the compression displacement of the rib pillar at the cusp.

The Taylor series expansion is used for the balance surface Eq. (14) at the cusp. After variable substitution, the cusp mutation standard form of balance surface equation that uses X as the variable and a and b as the control parameters is written as

$$\left.\begin{aligned} &X^3 + aX + b = 0 \\ &a = \frac{6}{k_1(k_2m+1)^2}(\eta - 1) \\ &b = \frac{6}{k_1k_2m(k_2m+1)^2}(1 + k_2m\eta - \xi) \end{aligned}\right\} \quad (17)$$

where

$$\left.\begin{aligned} X &= \left(\frac{u-u_1}{u_1}\right) \\ \eta &= \frac{\eta_1}{\eta_2} = \frac{24EI}{l^3\lambda k_2 m \exp\left(-\dfrac{k_2 m+1}{k_2 m}\right)} \\ \xi &= \frac{ql}{\lambda u_1 \exp\left(-\dfrac{k_2 m+1}{k_2 m}\right)} \\ \eta_1 &= \frac{24EI}{l^3} \\ \eta_2 &= \lambda k_2 m \exp\left(-\frac{k_2 m+1}{k_2 m}\right) \end{aligned}\right\} \quad (18)$$

Figure 7 shows the cusp catastrophe model described by the balanced curved surface of the folding wing. It shows that the three-dimensional coordinates are the control parameters (a, b) and state variables. When the control parameters (a, b) change continuously along the BB' direction, the state variable X changes continuously, and the support system does not change suddenly. However, when the control parameters change continuously along the AA' direction, the state variable X suddenly increases, and the supporting system is unstable and damaged close to the edge of the folding wing.

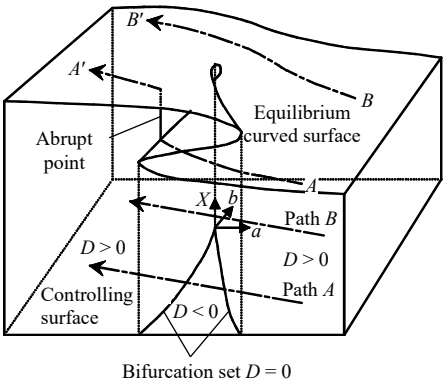

Fig. 7 Equilibrium surface of cusp-catastrophe model

X is used as a variable to derive the standard form of the equilibrium curved surface equation, the critical state equation of the support system can be written as

$$3X^2 + a = 0 \quad (19)$$

Combining Eqs. (16) and (17) can obtain the equation of the function bifurcation set of the support system, that is, the projection of the crease of the balance surface on the a−b plane is

$$D = 4\beta^3(\eta-1)^3 + 27\frac{\beta^2}{(k_2 m)^2}(1+k_2 m-\xi)^2 = 0 \quad (20)$$

where

$$\beta = \frac{6}{k_1(k_2 m+1)^2} \quad (21)$$

5.3 Instability mechanism of support system

Figure 7 shows that the equilibrium point of the system may cross the function bifurcation set when a<0. According to Eq. (17), the instability conditions of supporting system can be derived as

$$\eta = \frac{24EI}{l^3\lambda k_2 m \exp\left(-\dfrac{k_2 m+1}{k_2 m}\right)} \leqslant 1 \quad (22)$$

It can be seen from Eq. (22) that the instability and failure of the roof−pillar support system under backfilling mining are determined by the stope span l, the roof thickness d, the elastic modulus E of the roof, the initial stiffness of the rib pillars λ and the action coefficient of the filling body k_2, but not other parameters. When the elastic modulus and thickness of the roof are much larger, and the stope span l, initial stiffness of the rib pillars λ are much smaller, making a large stiffness ratio of the support system, and the support system is more stable. After the stope is filled in time, the lateral pressure of the filling body on the rib pillars cause the action coefficient of the filling body to decrease, thus the stiffness ratio η and stability of the supporting system are increased.

When D = 0 in the supporting system, there are 3 real roots in Eq. (17), among them, 2 of them are in stable states and another is in the unstable state. At this time, the control parameters (a, b) must have a sudden change when they cross the function bifurcation set. Therefore, D = 0 is a sufficient condition for the instability of the support system. When the control parameters (a, b) cross the right branch (b>0), the state parameter X of the support system does not change at this time. When the stope support system is unstable, its deformation appears to increase suddenly, and the control parameters (a, b) cross the right branch of the function bifurcation set (b<0), that is

$$b = \frac{6}{k_1 k_2 m(k_2 m+1)^2}(1+k_2 m\eta-\xi) < 0 \quad (23)$$

Therefore, the necessary and sufficient conditions of the instability in supporting system can be summarized as

$$\left.\begin{aligned} D &= 4\beta^3(\eta-1)^3 + 27\frac{\beta^2}{(k_2 m)^2}(1+k_2 m-\xi)^2 = 0 \\ b &= \frac{6}{k_1 k_2 m(K_2 m+1)^2}(1+k_2 m\eta-\xi) < 0 \\ \eta &\leqslant 1 \end{aligned}\right\} \quad (24)$$

It can be seen from Eq. (24) that under the condition of certain rock mass mechanical parameters, the stability of the rib pillar−roof support system under the action of the filling body is affected by the stope structure parameters, the overburden q and the action coefficients k_1 and k_2 of the filling body. Among them, the stope structure parameters include stope span l, rib pillar height H, rib pillar width B, and roof thickness d.

5.4 Influence of stope structure parameters on stope stability

For a specific mine, the mechanical parameters and external load of the rock mass are determined, so the stability of the stope mainly depends on the structural parameters. Based on the material parameters of a specific supporting project, taking the stope span l (50−70 m with the interval of 1 m), the height of the rib pillars H (70−90 m with the interval of 1 m), the width of the rib pillars B (15−25 m with the interval of 0.5 m), and the roof thickness d (8−12 m, with the interval of 0.2 m) are independent variables, the variations of controlling parameters at the unfilled state (a_0, b_0) and the filled state (a, b) are analyzed. Here the, impacts of stope parameters on a_0 and a are shown. Fig.8 is the relationship of stope span l and the controlling parameters a_0 and a. Fig.9 shows the relationship of rib pillar height H and the controlling parameters a_0 and a. Figs. 10 and 11 are the correlation among rib pillar width B, roof thickness d and the controlling parameters a_0 and a.

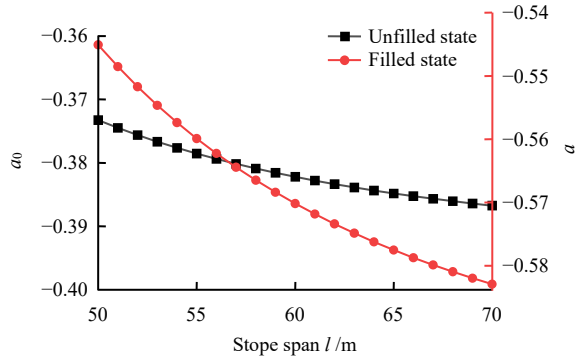

Fig. 8 Relationships between stope span and a_0, a

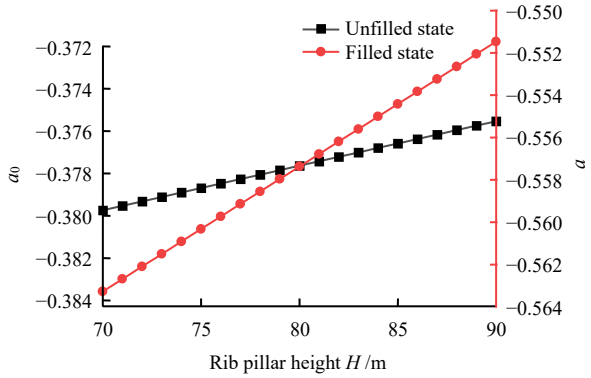

Fig. 9 Relationships between rib pillar height and a_0, a

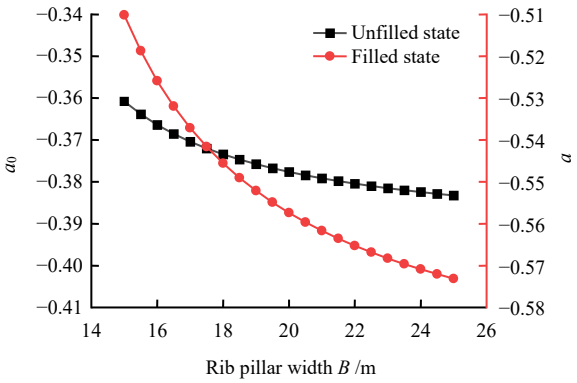

Fig. 10 Relationships between rib pillar width and a_0, a

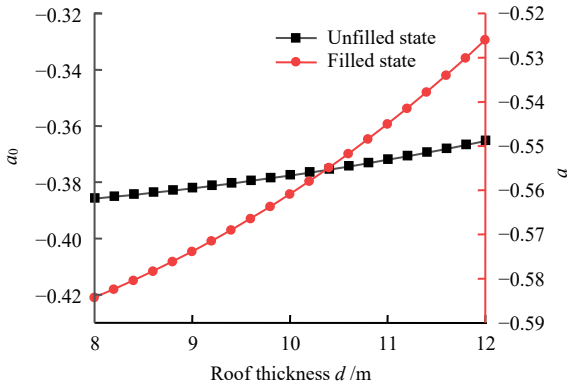

Fig. 11 Relationships between roof thickness and a_0, a

The variation law between stope structure parameters and control parameters will be changed due to the addition of filling bodies (see Figs. 8−11). In order to analyze the influence of stope structure parameters on stope stability under different conditions, applying the method proposed by Xia et al.[22] in the slope problem, the sensitivity analyses of the stope structure parameters at the filling and filling states on the stability of rib pillars−roof support system are carried out. It shows in Figs. 12 and 13 that the sensitivity coefficients of stope span, roof thickness, rib pillar height, and rib pillar width are 2.03, 2.77, 0.89, and 1.79, respectively for the unfilled state. At the filled state, the sensitivity coefficients of stope span, roof thickness, rib

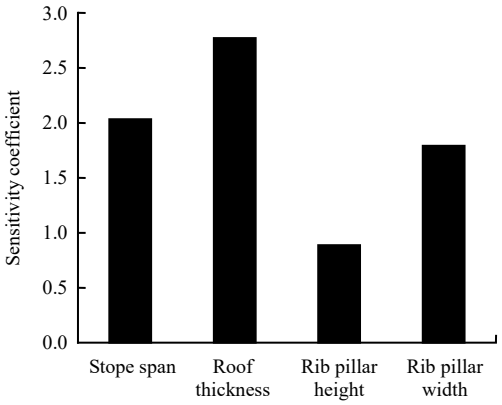

Fig. 12 Histogram of sensitivity coefficient in the unfilled state

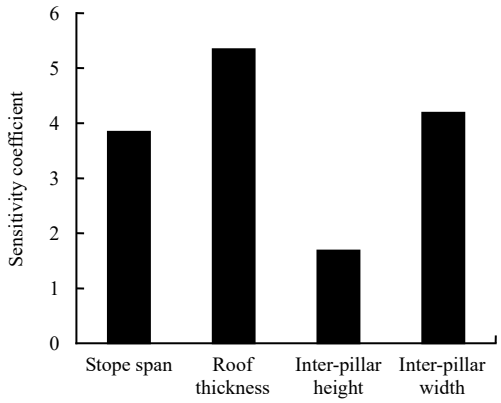

Fig. 13 Histogram of sensitivity coefficients in the filled state

pillar height, and rib pillar width are 3.84, 5.34, 1.68 and 4.19, respectively. Applying the same solution method, the same variation law can be found for the sensitivity of b_0 and b.

In summary, when the roof−rib pillar support system is at the unfilled state, the stope parameters that play a major role in controlling the stability of the roof−rib pillar support system are roof thickness, stope span, width and height of rib pillars. This is in consistent with the results of Xu et al.[23], proving the reliability of this research. When the roof−rib pillar support system is at the filling state, the stope parameters that play a major role in controlling the stability of the roof−rib pillar support system are the thickness of the roof, the width of the rib pillar, the stope span, and the height of the rib pillar. The main reason for the above phenomenon is that the stress state of the rib pillars is changed due to the addition of filling bodies, which improves the bearing capacity of the rib pillars, making the width of the rib pillars play a more important role in controlling the stability of the stope. In the process of optimizing the structural parameters of the stope filling, the above analysis results can be used.

6 Engineering application

6.1 Project background

A metal mine located in northeastern China is selected in the studies. The landform of the mining area is hills and mountainous, and the overall terrain is high in the east and low in the west. The strata in the mining area mainly includes the Yingtaoyuan metamorphic rock formation of the Anshan Group of Archean, the Langzishan metamorphic rock formation of the Liaohe Group of the Lower Proterozoic, and the alluvial strata of the Quaternary of Cenozoic. The Yingtaoyuan metamorphic rock Formation of the Anshan Group is an ore-bearing strata in this region, and the ore bodies occur in the chlorite quartz schist. Most of the faults in this region are covered by the Quaternary system, and the signs of tectonic movement are not obvious. The mining area is close to the high-tech developmental zone, and the backfill mining method is applied. In the middle of the mining section, a stope is set along the strike of the ore body. The stope is divided into two−step mining blocks, and the one−step mining and the two−step mining are arranged at intervals. A rib pillar with a width of 20 m is left between adjacent ore blocks perpendicular to the strike of the ore body. The cement filling is carried out immediately after the completion of the one−step stoping, and then the two−step stoping is carried out and filled with tailings. The material parameters in the stope is shown in Table 3. When the mine is mined to the middle section of −860 m, in order to support the filling body above the middle section of −780 m and the weight of rocks in the collapse zone, a certain thickness of roof must be reserved in the middle section of −780 m. As a result, a roof−rib pillar support system is formed in the stope. If the support system suffers large-scale instability and damage, it will seriously affect the safety production at the −860 m level.

6.2 Theoretical analysis

In order to reasonably determine the roof thickness d required for mining in the middle section of −860 m, the roof thickness d is used as an independent variable (e.g., 8−12 m, with an interval of 0.2 m). According to Eq. (24), the effects of thickness d on the stability of the support system in the unfilled and filled states are studied respectively, as shown in Table 4.

It can be seen from Table 4 that the stiffness ratio of the support system decreases with the decrease of the roof thickness when other parameters are constant, meaning that the support system is more likely to be instability. In the unfilled state, when the roof thickness d decreases from 11.6 m to 11.4 m, D_0 changes from −0.002 1 to

Table 3 Material parameters of the stope

E /GPa	E_0 /GPa	μ	Stope span l /m	Rib pillar height H /m	Rib pillar width B /m	Overburden rock density ρ /(kg • m^{-3})	Filling body density ρ_0 /(kg • m^{-3})	Mining depth Z /m
24	27	0.21	60	80	20	2 700	1 970	860

Table 4 Relationships between roof thickness and stability of support system

Roof thickness d /m	Filled state				Unfilled state			
	Stiffness ratio η	b	D	State	Stiffness ratio η_0	b_0	D_0	State
8.0	0.040 3	−0.182 8	0.104 9	Instability	0.021 8	−0.102 4	0.056 8	Instability
8.2	0.043 4	−0.181 0	0.094 1	Instability	0.023 4	−0.101 8	0.054 3	Instability
8.4	0.046 7	−0.179 0	0.082 9	Instability	0.025 2	−0.101 1	0.051 8	Instability
8.6	0.050 1	−0.176 9	0.071 3	Instability	0.027 0	−0.100 3	0.049 1	Instability
8.8	0.053 7	−0.174 7	0.059 3	Instability	0.029 0	−0.099 6	0.046 4	Instability
9.0	0.057 4	−0.172 4	0.047 0	Instability	0.031 0	−0.098 8	0.043 5	Instability
9.2	0.061 3	−0.170 1	0.034 3	Instability	0.033 1	−0.098 0	0.040 5	Instability
9.4	0.065 4	−0.167 6	0.021 4	Instability	0.035 3	−0.097 1	0.037 5	Instability
9.6	0.069 7	−0.165 0	0.008 1	Instability	0.037 6	−0.096 2	0.034 3	Instability
9.8	0.074 1	−0.162 3	−0.005 5	Stability	0.040 0	−0.095 3	0.031 0	Instability
10.0	0.078 8	−0.159 4	−0.019 3	Stability	0.042 5	−0.094 3	0.027 7	Instability
10.2	0.083 6	−0.156 5	−0.033 3	Stability	0.045 1	−0.093 2	0.024 2	Instability
10.4	0.088 6	−0.153 5	−0.047 5	Stability	0.047 8	−0.092 2	0.020 7	Instability
10.6	0.093 8	−0.150 3	−0.061 8	Stability	0.050 6	−0.091 1	0.017 1	Instability
10.8	0.099 2	−0.147 0	−0.076 3	Stability	0.053 5	−0.089 9	0.013 4	Instability
11.0	0.104 8	−0.143 6	−0.090 9	Stability	0.056 6	−0.088 8	0.009 6	Instability
11.2	0.110 6	−0.140 0	−0.105 5	Stability	0.059 7	−0.087 5	0.005 8	Instability
11.4	0.116 7	−0.136 4	−0.120 0	Stability	0.063 0	−0.086 2	0.001 9	Instability
11.6	0.122 9	−0.132 6	−0.134 6	Stability	0.066 3	−0.084 9	−0.002 1	Stability
11.8	0.129 4	−0.128 6	−0.148 9	Stability	0.069 8	−0.083 5	−0.006 1	Stability
12.0	0.136 1	−0.124 5	−0.163 2	Stability	0.073 4	−0.082 1	−0.010 2	Stability

Note: η_0 and D_0 are control parameter and function bifurcation of the support system at the unfilled state.

0.001 9, which means that the control parameters (a_0, b_0) cross the function bifurcation set. Thus the supporting system is unstable and damaged because it satisfies the necessary and sufficient conditions for instability in Eq. (24). Meanwhile, the roof thickness is reduced from 9.8 m to 9.6 m in the filling state, and the support system will be unstable and damaged. Compared with the unfilled state, the addition of the filling body can significantly reduce the critical instability thickness (15.5%) of the roof, thereby increasing the recovery rate of mines. Considering that the backfill mining method is planned in this project and the timely filling is required during the actual mining process, the critical instability thickness of the roof in the support system is set as 9.8 m.

6.3 Verification of the numerical simulation

Considering that the geological conditions of the mining area and the occurrence conditions of the ore body are very complicated, the numerical simulation software FLAC^{3D} is used to verify the theoretical analysis results. According to the geological survey section map of the mining area, the rock masses with similar lithology are merged and simplified, and there are six types of lithology including iron ore, carbonaceous phyllite, chlorite phyllite, chlorite quartz schist, gneissic granite etc. According to the geological survey and rock mechanical test, combined with the classification of engineering rock mass, the mechanical strength parameters of different rock masses are initially determined (see Table 5).

Table 5 Physical and mechanical parameters of rock mass

Types	Density /(kg • m^{-3})	Deformation modulus /GPa	Poission's ratio	Cohesion /MPa	Frictional angle /(°)	Tensile strength /MPa
Fault F1	2 020	0.50	0.38	0.07	22.00	0.09
Gneissic granite	2 800	18.00	0.23	1.70	44.00	1.44
Carbonaceous phyllite	2 780	12.00	0.27	1.20	39.28	1.14
Chlorite quartz schist	2 790	17.00	0.24	1.60	42.98	1.39
Iron ore	3 410	30.00	0.21	2.00	47.07	1.57
Chlorite phyllite	2 770	10.00	0.29	1.00	39.95	0.93
Filling body	1 970	0.36	0.28	0.24	31.00	0.33

The three-dimensional numerical model of the mining area is shown in Fig.14. In order to eliminate the influence of boundary effect, the dimension of the model is 3 400.0 m×2 071.2 m×420.0 m (length×width×height), with a total of 920 012 meshes. The Mohr−Coulomb constitutive relationship is used in the model, and the instability and failure behavior of the stope is studied only considering the self-weight stress field. To obtain the real stress field and displacement field in the middle section of −860 m before the excavation of the stope, the simulation steps strictly follow the actual mining sequence

and immediately backfill, and each step is calculated to a balance state.

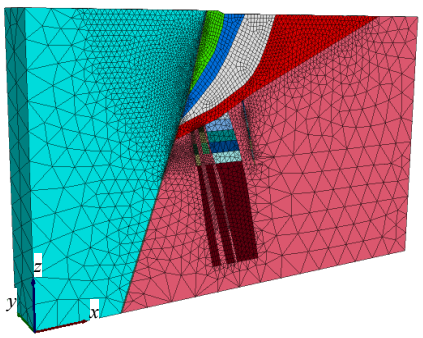

Fig. 14 Three-dimensional numerical calculation model

Mining activities will cause deformation and displacement of surrounding rock, and stope instability is often accompanied by roof falling. For the roof−rib pillar support system, the failure of the rib pillars that play the main supporting role causes the structural instability of the supporting system. Fig.15 shows the relationship between the displacement D_c at the center of the rib pillar and the roof thickness d. It can be seen from Fig.15 that the displacement D_c at the center of the rib pillar increases with the decrease of the roof thickness d. When the roof thickness is reduced from 12.5 m to 9.0 m, the displacement D_c of the rib pillar at the center slowly increases. When the roof thickness d decreases from 9.0 m to 8.5 m, the displacement D_c of the rib pillar at the center increases sharply with the amount of 7.09 cm, which is 177.75% of the displacement of the rib pillar at the center with d = 9.0 m. The rib pillar is in the unstable state, and the structural instability of roof−rib pillar support system occurs. When the stope is filled in time, the critical instability thickness of the stope roof is 9.0 m, which has a good match with the previous theoretical analysis with the critical instability thickness of 9.8 m. The numerical simulation results verify that the theoretical derivation is correct.

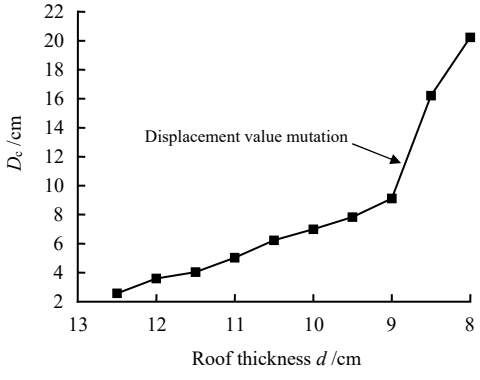

Fig. 15 Relationship between roof thickness and D_c

7 Conclusions

The purpose of this paper is to study the failure characteristics of the roof−rib pillar support system under backfill mining. The Weibull distribution is applied to describe the stress−strain relationship curve of the rib pillar under the action of the backfill. Based on a simplified mechanical model, the catastrophe theory is used to analyze the damage mechanism of the support system. The sensitivity of stope structure parameters that affect the stability of the support system is investigated and the following conclusions are drawn.

(1) When the mechanical parameters of the rock mass are fixed, the stability of the rib pillar−roof support system under backfill mining is affected by the stope structure parameters (e.g., the roof thickness, the stope span, the inter pillar width and the height of the rib pillar), the overlying load and the confining pressure of the filling body. The filling body will reduce the stiffness ratio of the support system, thereby improving the stability of the stope.

(2) During the adjustment of the stability of the roof−rib pillar support system, if the stope is in an unfilled state, the optimization sequence should be roof thickness, stope span, rib pillar width and the height of the rib pillar. If the stope is in the filling state, the optimization sequence should be roof thickness, rib pillar width, stope span, and rib pillar height. For a backfill stope, the width of the rib pillars play a more important role in controlling the stability of the stope.

(3) By applying the theoretical derivation to the supporting project, finally the roof thickness is selected as 9.8 m. The theoretical results are verified by numerical simulation. The results show that the critical instability thickness of the roof is 9.0 m when the stope is filled in time. The numerical simulation results have a good match with the theoretical results, proving that the theoretical derivation is correct.

References

[1] LI Xi-bing, LIU Bing. Review and exploration on the current situation of filling mining in hard rock mines[J]. Gold Science and Technology, 2018, 26(4): 492−502.

[2] LIU Wu-tuan, ZHANG Hai-lei, WANG Cheng-cai, et al. Analysis of safety technology factor of advanced mining in Lijiagou mine area[J]. Metal Mine, 2015(3): 169−172.

[3] XIE Xue-bin, LI Jian-kun, DONG Xian-jiu, et al. Research on stability of cemented backfill-roof system[J]. Rock and

Soil Mechanics, 2018, 39(11): 4183−4190.

[4] XU Wen-bin, SONG Wei-dong, CAO Shuai, et al. Stopes stability in underground mine and its control technique[J]. Journal of Mining and Safety Engineering, 2015, 32(4): 658−664.

[5] VERMA C P, PORATHUR J L, THOTE N R, et al. Empirical approaches for design of web pillars in highwall mining: review and analysis[J]. Geotechnical and Geological Engineering, 2014, 32(2): 587−599.

[6] WANG Xiao-jun, FENG Xiao, ZHAO Kui, et al. Study of critical thickness of roof of level pillar stoping under multifactor influence[J]. Rock and Soil Mechanics, 2013, 34(12): 3505−3512.

[7] CHEN Qing-fa, GU De-sheng, ZHOU Ke-ping, et al. Analysis of catastrophe theory for artificial pillar instability in symmetric synergistic mining[J]. Journal of Central South University (Science and Technology), 2012, 43(6): 2338−2342.

[8] ZHAO Yan-lin, WU Qi-hong, WANG Wei-jun, et al. Strength reduction method to study stability of goaf overlapping roof based on catastrophe theory[J]. Chinese Journal of Rock Mechanics and Engineering, 2010, 29(7): 1424−1434.

[9] XIA Kai-zong, CHEN Cong-xin, SONG Xu-gen, et al. Analysis of the mechanism of catastrophic failure of gypsum mine top under relative humidity[J]. Rock and Soil Mechanics, 2018, 39(2): 589-597.

[10] REN Hong-gang, WANG Xu-guang, TAN Zhuo-ying, et al. Construction of three-dimensional mechanical model for creep and catastrophe of goaf group and accurate prediction of its stability[J]. Journal of Central South University (Science and Technology), 2019, 50(12): 3114−3126.

[11] XU Heng, WANG Yi-ming, WU Ai-xiang, et al. A computational model of safe thickness of roof under filling body based on cusp catastrophe theory[J]. Chinese Journal of Rock Mechanics and Engineering, 2017, 36(3): 579−586.

[12] QI Kuan. Study on performance of cemented backfill materials with unclassified tailings and stability of stope surrounding rock in Yongping copper mine[D]. Beijing: University of Science and Technology Beijing, 2018.

[13] XU Xiao-dong, SUN Guang-hua, YAO Xu-long, et al. A cusp catastrophe warning model for instability of backfill based on energy dissipation and release[J]. Rock and Soil Mechanics, 2020, 41(9): 3003−3012.

[14] ZHU X J, GUO G L, FANG Q. Coupled discrete element-finite difference method for analyzing subsidence control in fully mechanized solid backfilling mining[J]. Environmental Earth Sciences, 2016, 75(8): 1−12.

[15] KOSTECKI T, SPEARING A J S. Influence of backfill on coal pillar strength and floor bearing capacity in weak floor conditions in the Illinois Basin[J]. International Journal of Rock Mechanics and Mining Sciences, 2015, 76: 55−67.

[16] SONG Wei-dong, REN Hai-feng, CAO Shuai. Interaction mechanism between backfill and rock pillar under confined compression condition[J]. Journal of China University of Mining & Technology, 2016, 45(1): 49−55.

[17] CAO Rui-lang, HE Shao-hui, WEI Jing, et al. Study of modified statistical damage softening constitutive moded for rock considering residual strength[J]. Rock and Soil Mechanics, 2013, 34(6): 1652−1667.

[18] DONOVAN J G, KARFAKIS M G. Design of backfilled thin-seam coal pillars using earth pressure theory[J]. Geotechnical and Geological Engineering, 2004, 22(4): 627−642.

[19] TESARIK D R, SEYMOUR J B, YANSKE T R. Longterm stability of a backfilled room-and-pillar test section at the Buick mine, Missouri[J]. International Journal of Rock Mechanics and Mining Sciences, 2009, 46: 1182−1196.

[20] TAN Yu-ye, YU Xin, SONG Wei-dong, et al. Experimental study on combined pressure-bearing mechanism of filling body and surrounding rock[J]. Journal of Mining & Safety Engineering, 2018, 35(5): 1071−1076.

[21] LONG Yu-qiu, BAO Shi-hua. Structural mechanics[M]. Beijing: Higher Education Press, 2008: 277−284.

[22] XIA Kai-zong, CHEN Cong-xin, LU Zu-de, et al. Analysis of sensitivity factors to stability of inter-beddings of soft and hard rock slope[J]. Journal of Wuhan University of Technology (Transportation Science and Engineering), 2013, 37(4): 729−733.

[23] XU Xiao-ding, ZHOU Yue-jin, PANG Shun. Analysis of catastrophic instability of plastic supporting system in old goaf of gypsum mine[J]. Chinese Journal of Rock Mechanics and Engineering, 2018, 37(11): 2548−2555.